MODELLING OF MULTI-PHASE FLUID FLOW WITH VOLUME FRACTION PAST A PERMEABLE STRETCHING VERTICAL CYLINDER AND ITS NUMERICAL STUDY

D. DEY and B. CHUTIA

†Department of Mathematics, Dibrugarh University, Dibrugarh-786004, India.
E-mail: debasish41092@gmail.com, chutia.barbie10@gmail.com

***Abstract*---A steady two-dimensional mixed convective multi-phase fluid (base fluid containing dust particles) flow past a vertical stretching cylinder in presence of volume fraction has been investigated. The surface of the cylinder is embedded by a porous medium in presence of a non-uniform source/sink. Governing partial differential equations of the problem for both fluid and dust phases are converted into ordinary differential equations using similarity transformations. MATLAB built-in bvp4c solver technique is used to solve the resulting non-linear differential equations. The results are presented in graphical forms for various values of flow parameters.**

***Keywords*---Dusty fluid, stretching vertical cylinder, volume fraction, Porous medium, Heat source/sink.**

I. INTRODUCTION

The study of dusty fluid or multiphase fluid flow is of keen interest to researchers due to its wide range of applications in real-world fluid flow problems. Two-phase flow problems are important in several fields such as in engineering, industries, etc. Firstly, the study of the stability of laminar flow of dusty fluids has been discussed by Saffman (1962). Chakrabarti (1977) has studied the boundary layer flow of a dusty fluid.

Mucoglu and Chen (1975) have studies the mixed convective flow over a vertical cylinder. Later, Wang (1988) has investigated the effect of heat transfer on viscous fluid flow past a stretching cylinder. Recently, investigations have been done on the study of fluid flow over stretching surfaces by Prasad *et al.* (2020) and Vaidya *et al.* (2021). The numerical solution of the fluid flow with heat transfer effects along a vertical hollow cylinder has been carried out by Chang (2008). Nayfeh and Vajravelu (1992) have investigated conducting dusty fluid flow over a stretching sheet. Gireesha *et al.* (2913) have discussed the thermal diffusion problem on two-phase fluid flow over a stretching surface without volume fraction. Recently, Prasad *et al.* (2016a) have investigated the study of two-phase fluid past a slender cylinder. Study of heat and mass transfer past a porous medium has been discussed by Vaidya *et al.* (2020).

Gupta and Gupta (1990) have investigated the effect of heat transfer of a dusty visco-elastic fluid past a channel with volume fraction. Singh and Singh (2002) have studied the flow problem of dusty fluid through two vertical parallel plates in presence of volume fraction. In recent years, Dey with his co-worker has studied the two-phase fluid flow problems using volume fraction (Dey, 2016a; Dey and Chutia, 2020). Also, study of two phases of fluid flow through a porous medium has been studied by Dey (2016b).

Manjunatha *et al.* (2014) have obtained the effect of heat transfer over a stretching cylinder under the influence of a non-uniform source/sink by neglecting volume fraction. However, this assumption is not justified for higher fluid density or large mass fraction of the dust particles. Extension of the work of Manjunatha *et al.* (2014) have been done and investigated the effect of heat transfer in a dusty fluid flow over a vertical stretching cylinder under the influence of volume fraction. The main objective of this paper is to calculate the rate of heat transfer and coefficient of skin friction of two-phase fluid flow as it has a wide range of applications in engineering, controlling pollution, cooling effects and many more. The problem has been investigated for two cases: PST and PHF where PST (Prescribed surface temperature) usually suitable for heating and PHF (Prescribed surface heat flux) for cooling. Also, the buoyancy effects within the boundary layer formed by the moving cylinder vertically are highly significant for laminar flow. The resulting non-linear equations are simplified using similarity transformations. Then, numerical solutions have been formulated using MATLAB built-in solver Bvp4c as it controls the true error in the calculation (Dey and Hazarika, 2020; Dey and Borah, 2020). The effects of velocity and temperature have been obtained graphically and the flow has been discussed in a tabular form.

II. MATHEMATICAL FORMULATION OF THE PROBLEM

A two-dimensional, steady flow of an incompressible conducting two-phase fluid flow (base fluid with consisting dust particles) past a stretching cylinder with radius a has been taken into account. The z-axis is measured along the axis of the cylinder and the r-axis is measured along the radial direction as shown in Fig. 1. The surface of the stretching cylinder is considered porous and a magnetic field of uniform B_0 has been applied along the radial direction.

Following assumptions are taken into account in the governing equations:

- The dust particles having zero conductivity with round and uniform sizes.
- Low magnetic Reynolds number (for smaller conductivity) helps to neglect induced magnetic field effects.

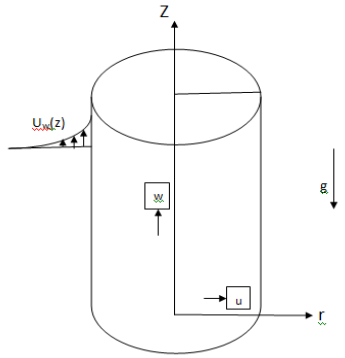

Fig. 1: Flow configuration of the problem.

- The system is considered with uniform distribution of dust particles.

Considering these assumptions, the governing equations for the flow in cylindrical coordinates are as follows:

$$\frac{\partial w}{\partial z}+\frac{1}{r}\frac{\partial (ru)}{\partial r}=0 \tag{1}$$

$$(1-\phi)\left(w\frac{\partial w}{\partial z}+u\frac{\partial w}{\partial r}\right)=(1-\phi)\left[\vartheta\left(\frac{\partial^2 w}{\partial r^2}+\frac{1}{r}\frac{\partial w}{\partial r}\right)+g\beta'^{(T-T_\infty)}-\frac{\sigma B_0^2 w}{\rho}-\frac{\vartheta w}{k_p}\right]+\frac{KN}{\rho}\left(w_p-w\right) \tag{2}$$

$$\frac{Nm}{\rho}\left(w_p\frac{\partial w_p}{\partial z}+u_p\frac{\partial w_p}{\partial r}\right)=\phi\left[\vartheta\left(\frac{\partial^2 w}{\partial r^2}+\frac{1}{r}\frac{\partial w}{\partial r}\right)+g\beta'^{(T-T_\infty)}-\frac{\sigma B_0^2 w}{\rho}-\frac{\vartheta w}{k_p}\right]-\frac{KN}{\rho}\left(w_p-w\right) \tag{3}$$

$$\frac{Nm}{\rho}\left(w_p\frac{\partial u_p}{\partial z}+u_p\frac{\partial u_p}{\partial r}\right)=\phi\left[\vartheta\left(\frac{\partial^2 u}{\partial r^2}+\frac{1}{r}\frac{\partial u}{\partial r}\right)-\frac{\sigma B_0^2 u}{\rho}-\frac{\vartheta u}{k_p}\right]-\frac{KN}{\rho}\left(u_p-u\right) \tag{4}$$

$$\rho C_p\left[w\frac{\partial T}{\partial z}+u\frac{\partial T}{\partial r}\right]=\frac{k}{r}\frac{\partial}{\partial r}\left(r\frac{\partial T}{\partial r}\right)+\frac{NC_p}{\tau_T}\left(T_p-T\right)+\frac{N}{\tau_v}\left(w_p-w\right)^2-q''' \tag{5}$$

$$NC_m\left[w_p\frac{\partial T_p}{\partial z}+u_p\frac{\partial T_p}{\partial r}\right]=\frac{-NC_p}{\tau_T}\left(T_p-T\right) \tag{6}$$

$$\frac{\partial}{\partial z}\left(w_p\rho_p\right)+\frac{1}{r}\frac{\partial}{\partial r}\left(r\rho_p u_p\right)=0 \tag{7}$$

where

$$q'''=\left(\frac{kU_w(z)}{z\vartheta}\right)\left[A^*(T_w-T_\infty)f'(\eta)+B^*(T-T_\infty)\right].$$

The boundary conditions for the flow problem are as follows:

$$u=U_w(z),\ u=0 \text{ as } r=a\ ;$$

$$w\to 0,\ \ w_p\to 0,\ u_p\to u,\ \rho_p\to w_p\ \text{ as } r\to\infty$$

$$T=T_w=T_\infty+A\left(\frac{z}{l}\right)^2 \text{ at } r=0\ (PST\ case);$$

$$-k\frac{\partial T}{\partial r}=q_w=D\left(\frac{z}{l}\right)^2 \text{ at } r=0\ (PHF\ case)$$

$$T\to T_\infty,\quad T_p\to T_\infty \quad as \quad y\to\infty$$

III. METHOD OF SOLUTION:

The governing equations are transformed into the corresponding ordinary differential equations; introducing the following similarity transformation (Manjunatha *et al.*, 2014):

$$\left.\begin{aligned} u&=-\frac{a}{r}\sqrt{\frac{\vartheta b}{l}}f(\eta), w=U_w(z)f'(\eta),\\ \eta&=\frac{r^2-a^2}{2a}\sqrt{\frac{U_w(z)}{\vartheta z}}, u_p=\frac{a}{r}\sqrt{\frac{\vartheta b}{l}}F(\eta),\\ w_p&=U_w(z)g(\eta),\ \ \rho_r=H(\eta),\\ \theta(\eta)&=\frac{T-T_\infty}{T_w-T_\infty},\ \theta_p(\eta)=\frac{T_p-T_\infty}{T_w-T_\infty}\end{aligned}\right\} \tag{8}$$

,

$T-T_\infty=A\left(\frac{z}{l}\right)^2\theta(\eta)$ (PST-Prescribed surface temperature);

$T_w-T_\infty=\frac{D}{k}\left(\frac{z}{l}\right)^2\sqrt{\frac{\vartheta}{c}}$ (PHF-Prescribed surface heat flux)

By substituting Eq. (8) in Eqs. (2-7), following nonlinear ordinary differential equations:

$$(1+2\eta\gamma)f'''+2\gamma f''-f'^2+ff''+Gr\theta-(Q+S)f'+l^*\beta\bar{\epsilon}H(g-f')=0 \tag{9}$$

$$l^*E(g^2+Fg')-(1+2\eta\gamma)f'''-2\eta\gamma f''-Gr\theta+(Q+S)f'+l^*\beta EH(g-f')=0 \tag{10}$$

$$l^*EFF'-\left(\frac{l^*E\gamma}{(1+2\eta\gamma)}\right)F^2+(1+2\eta\gamma)f''-(Q+S)f+l^*\beta EH(F+f)=0 \tag{11}$$

$$Prf\theta'+2\gamma\theta'+(1+2\eta\gamma)\theta''+NPra_1\left(\theta_p-\theta\right)+NPrEca_2(g-f')^2-A^*f'-B^*\theta=0 \tag{12}$$

$$F\theta_p'+b_1\left(\theta_p-\theta\right)=0 \tag{13}$$

The continuity equation of dust phase gives,

$$H.F=constant\ (C\ say) \tag{14}$$

where a prime denotes differentiation with respect to η.

$$Q=\frac{\sigma B_0^2 l}{b\rho},S=\frac{\mu l}{b\rho k_p},\bar{\in}=\frac{1}{1-\phi},E=\frac{1}{\phi},$$

$$\tau=\frac{m}{K},a_1=\frac{l}{\rho\tau_T b},\ a_2=\frac{l}{\rho\tau_v b},\Pr=\frac{\rho\vartheta C_p}{k},$$

$$b_1=\frac{C_p l}{\tau_T C_m b},Gr=\frac{g\beta(T_w-T_\infty)l^2}{b^2 z},\gamma=\sqrt{\frac{l\nu}{a^2 b}},$$

$$\beta=\frac{l}{\tau b},l^*=\frac{Nm}{\rho},Ec=\frac{bl^2}{AC_p}\ (PST),$$

$$Ec=\frac{kl^2 b^{\frac{3}{2}}}{AC_p}(PHF)$$

The transformed non-dimensional boundary conditions are as follows:

$$f=0,f'=1:\eta=0;$$

$$\theta=1\ \ (PST\ case);\ \theta'=-1:\eta=0\ (PHF\ case);$$

$$f'=\ g=0,F=f,H=\omega,\theta=\ \theta_p\to 0:\ \eta\to\infty$$

The quantities which are useful in engineering problems are the coefficient of skin friction and Nusselt number, which are defined as

$$C_f=\frac{\mu\left(\frac{\partial u}{\partial r}\right)_{r=a}}{\rho U_w^2},\qquad Nu_x=\frac{\mu\left(\frac{\partial T}{\partial r}\right)_{r=a}}{k(T_w-T_\infty)}$$

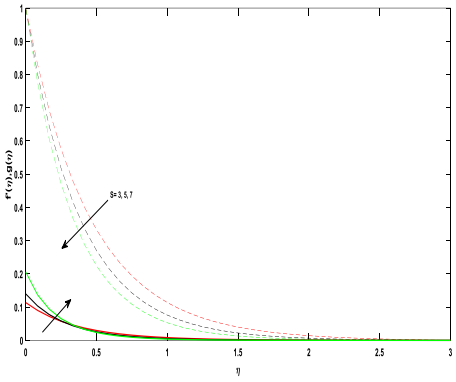

Fig. 2: Velocity distribution against displacement profile for PST.

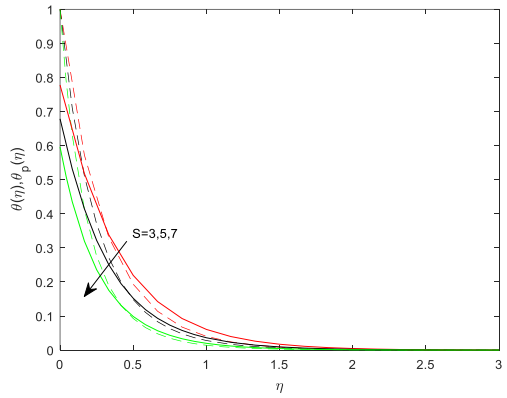

Fig. 3: Temperature distribution against displacement profile for PST.

Using the non-dimensional variables, the following dimensionless quantities are obtained

$$C_f Re_{xx}^{\frac{1}{2}} = f''(0), \quad Nu_x = -\sqrt{Re_x}\theta'(0) \ \ (PST\ case),$$

$$Nu_x = \frac{\sqrt{Re_x}}{\theta(0)} \qquad (PHF\ case)$$

IV. RESULTS AND DISCUSSION

In this paper, the non-linear Eqs. (9-14) are solved numerically with boundary conditions (8) using MATLAB built-in Bvp4c solver technique. The results have been presented using graphs and table. Figures and table are drawn using $S = 0.5$, $Q = 1$, γ=0.1, $Pr = 3$, $A^* = 0.2$, $B^* = 0.2$, $\beta = 0.5$, $\bar{\epsilon}$= 1.2, $E = 5$, $l^* = 1$. $N = 0.1$, $Ec = 0.01$, $C = 0.01$, $a_1 = 3$, $a_2 = 5$, $b_1 = 3$. In the figures, the solid line represents the properties of the fluid phase and the dashed line represents the properties of the dust phase.

Figure 2 depicts the graphs showing the effect of a permeable parameter (S) on both the velocity profiles of fluid and dust phases in case of PST. A deceleration in the velocity component of the fluid phase with the permeable parameter has been observed. This is because a decrease in permeability resists the fluid motion. Again, an inflexion point in the neighbourhood of the surface [0, 0.5] has been experienced, where there is no effect of S. Also, the velocity component of dust particles increases in the neighbourhood of the surface but the reverse effect is seen in the region far away from the surface.

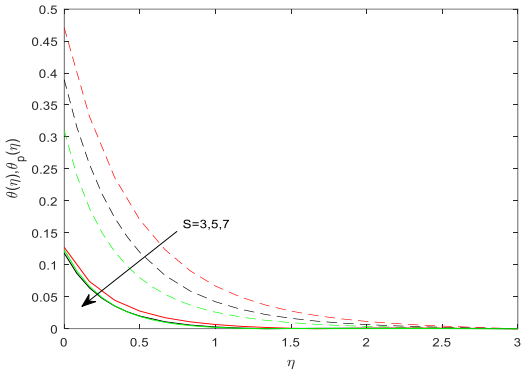

Fig. 4: Temperature distribution against displacement profile for PHF.

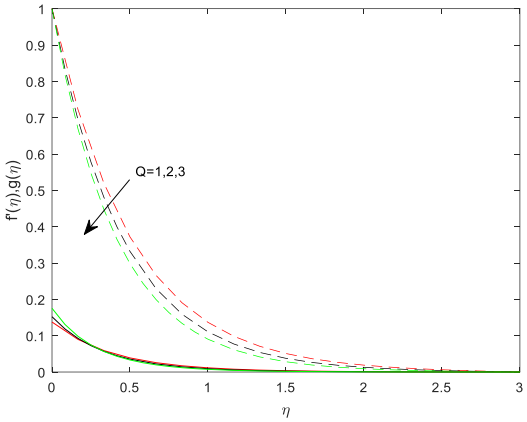

Fig. 5: Velocity distribution against displacement profile for PST.

Figures 3 and 4 illustrate the relationship between permeable parameter (S) and temperature profiles for both the phases in PST and PHF cases respectively. The temperature profiles for both the phases reduce until it reaches the thermal equilibrium stage with an increase in the values of S. That means that the porous medium resists the fluid flow and it also leads to the reduction in the temperature of both the phases.

Figure 5 describes the case of PST with the effects of a magnetic parameter (Q) on the velocity profile component of primary fluid motion of both phases. A rise in Q reduces the velocity profile of the fluid phase has been noticed. This is because the transverse magnetic field acting normal to the flow leads to a formation of opposing force known as Lorentz force which helps to decelerate the fluid motion. Further, the velocity of the dust phase increases near the stretching surface of the cylinder and the reverse effect occurs for the far surface. The values of Q are taken for a fully laminar flow.

Figures 6 and 7 are plotted to analyze the effect of a magnetic parameter (Q) on the temperature profile for both the phases in PST and PHF cases. From both the figures, it is seen that increasing values of the magnetic

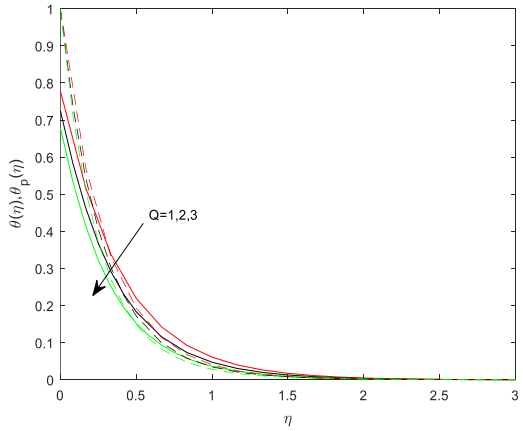

Fig. 6: Temperature distribution against displacement profile for PST.

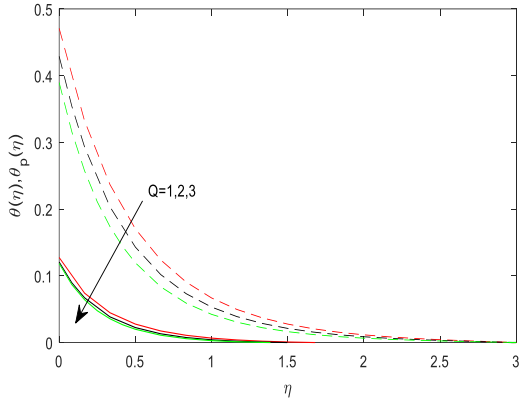

Fig. 7: Temperature distribution against displacement profile for PHF.

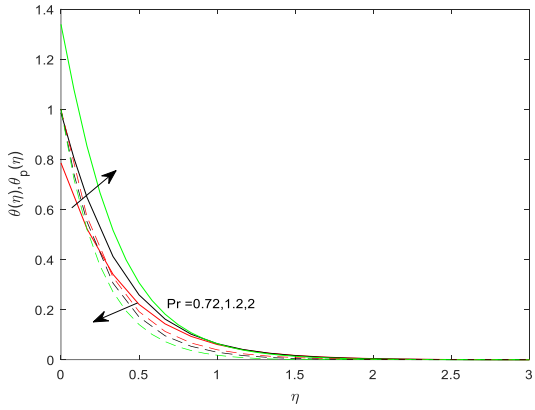

Fig. 8: Temperature distribution against displacement profile for PST.

parameter reduces the temperature profile for both phases in the respective two cases. As the Lorentz force slows down the flow process which leads to the decrement in the temperature profile.

Figures 8 and 9 depict the effects of Prandtl number (Pr) on the thermal boundary layer in both PST and PHF cases respectively for both phases. From both the figures, it is observed that with a rise in the values of Pr, the thermal boundary layer thickness reduces for the fluid phase. This means the temperature of the fluid

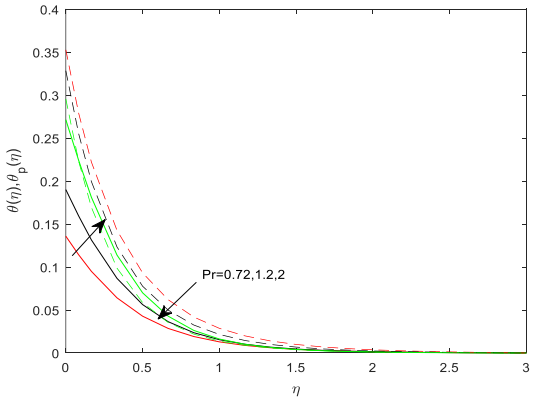

Fig. 9. Temperature distribution against displacement profile for PHF.

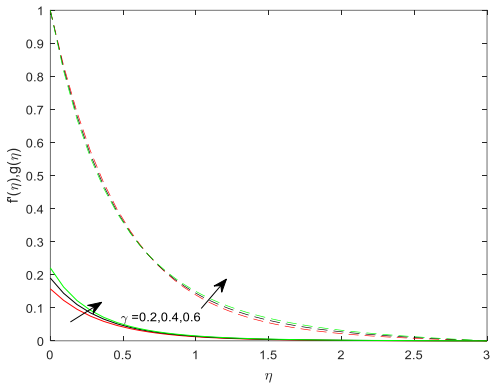

Fig. 10: Velocity distribution against displacement profile for PST.

phase in the case of gases ($\Pr = 0.72$) is less than viscous liquids ($\Pr > 1$). From the definition, the Prandtl number is inversely proportional to the thermal diffusivity so in order to that, the thermal diffusivity decreases with an increase in the values of Pr. It leads to the reduction in the temperature profile for the phases in both cases respectively. While the temperature of the dust phase increases as thermal diffusivity decreases.

Figure 10 illustrates the effect of the curvature parameter (γ) of the stretching cylinder on the velocity profile of both the phases in the PST case. From Fig. 10, it is seen that the velocities for both the phases increase with the curvature parameter.

Figures 11 and 12 depict the importance of relaxation parameter (β) on the temperature profile on both the phases in both cases respectively. From both the figures, it has been observed that for both PST and PHF cases, temperature profile increases with enhancement in the relaxation parameter (also known as fluid-particle interaction parameter). This means that with an increase in the value of β, the relaxation times of both the phases enhance the temperature profile.

Figure 13 depicts the effect of volume fraction parameter for both fluid and dust phase. A rise in the volume fraction parameter leads to decline in volume fraction ($\phi = 1/E$). It is seen that fluid motion is accelerated with diminishing values of volume fraction while opposite trend is seen for the dust phase.

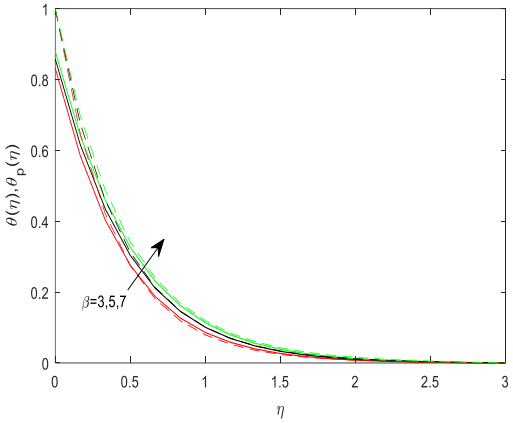

Fig. 11. Temperature distribution against displacement profile for PST.

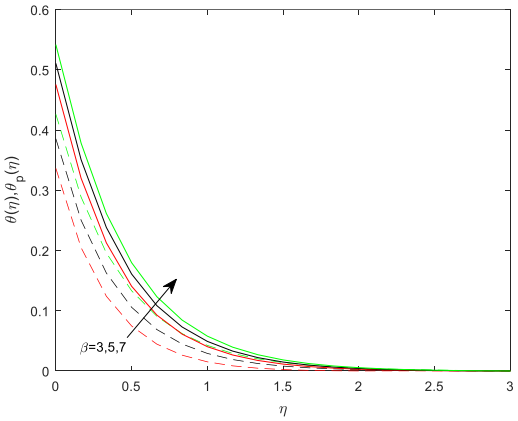

Fig. 12. Temperature distribution against displacement profile for PHF.

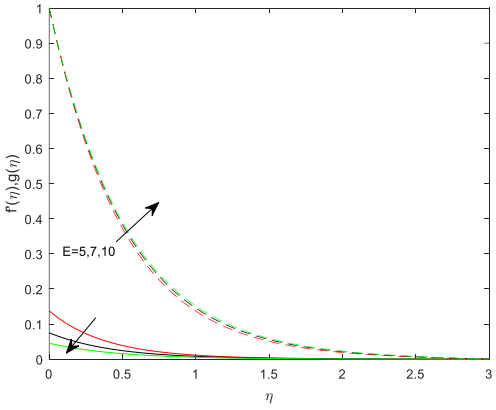

Fig. 13. Velocity distribution against displacement profile for PST.

Table I: Comparison and error analysis (Prasad *et al.*, 2016b) of the results for $-\theta'(0)$ for various values of Pr (neglecting Grashof number and volume fraction).

	(Manjunatha *et al.*, 2014)	Present study	Relative error
Pr	$-\theta'(0)$	$-\theta'(0)$	
1	1.3333	1.3333	0.0000
10	4.7964	4.7959	0.000104

Table II: The values of $f''(0)$, $-\theta'(0)$ and $\theta(0)$ for various values of A^*, B^*, Pr, E, Q, β, γ and S.

A^*	B^*	Pr	E	$-f''(0)$	$-\theta'(0)$	$-\theta(0)$
0.2				2.2163	6.0213	0.6701
0.4	0.2	3	5	2.2055	6.0373	0.6667
0.6				2.1936	6.0452	0.6603
	0.2			2.2163	6.0213	0.6701
0.2	**0.4**	3	5	2.2111	6.1304	0.7055
	0.6			2.2042	6.2319	0.7374
		3		2.2163	6.0213	0.6701
0.2	0.2	**5**	5	2.1225	6.9072	0.5734
		7		2.1046	7.9071	0.5376
			5	2.2163	6.0213	0.6701
0.2	0.2	3	**7**	2.2111	5.9591	0.6637
			10	2.2072	5.9131	0.6589
Q	*B*	γ	*S*	$-f''(0)$	$-\theta'(0)$	$-\theta(0)$
1				2.2163	6.0213	0.6701
1.5	0.1	0.1	0.5	2.3651	6.3885	0.8024
2				2.5042	6.7433	0.9325
	0			2.2151	6.0290	0.6696
1	**0.05**	0.1	0.5	2.2157	6.0251	0.6698
	0.1			2.2163	6.0213	0.6701
		0.1		2.2163	6.0213	0.6701
1	0.1	**0.4**	0.5	3.4521	9.0726	1.5364
		0.6		4.4553	11.2557	2.1441
			0.5	2.2163	6.0213	0.6701
1	0.1	0.1	**1**	2.3651	6.3885	0.8024
			1.5	2.5042	6.7433	0.9325

A comparison of this work with Manjunatha *et al.* (2014) has been shown by Table I. It shows the comparison of the previous paper and the present study for $-\theta'(0)$ for different values of Pr and relative error also has been calculated. It is noticed that the work is in good agreement.

Table II shows the relationship between various parameters with the magnitude of the coefficient of skin friction and the rate of heat transfer in both PST and PHF cases. It is seen that increasing values of A^*, B^*, Pr and E leads to the decrement in the magnitude of the coefficient of skin friction, while the rate of heat transfer rises in the PST case. In the case of PHF, as $Nu_x \propto \frac{1}{\theta}$ so the rate of heat transfer increases for the increasing values of A^*, Pr, E and reverse happens for the other parameters shown in the table.

V. CONCLUSION

Some of the conclusions from the above study are listed below:

- A raise in the values of volume fraction leads to the diffusion of heat for both the fluid and dust phases in PST.
- A boost in the values of the magnetic parameter leads to the declination in the velocity profile of the fluid phase and temperature profiles for both fluid and dust phase in both the cases of PST and PHF.
- In the PHF case, the thermal boundary layer thickness of fluid flow is higher than the PST case.
- Fluid velocity in all cases is more than that of the dust phase.

- The temperature profile of dust particles for both cases increases as the thermal diffusivity reduces while the reverse happens for the fluid phase.
- A raise in the values of curvature parameter, permeability parameter, flow and temperature-dependent source/sink parameter, and volume fraction and Prandtl number enhances the thermal diffusion rate (PST case).

NOMENCLATURE

(w, u) (m/s): Velocity components of the fluid phase, (w_p, u_p) (m/s): Velocity of dust phase, ρ (kg/m^3): Density of the fluid, ρ_P (kg/m^3): Density of dust phase, N (m^{-3}): Number density of the dust particles, $K(= 6\pi\mu d)$ (kg. ms^{-2}): Stoke's constant, β' (K^{-1}): Coefficient of expansion of the fluid, μ (Pa s): Dynamic viscosity of the fluid, d (m): Radius of the dust particles, B_0 (T): Magnetic field, k_p (N/A^2): Permeability of the porous medium, m (kg): Mass of the dust particles, σ (S/m): Electric conductivity of the fluid, ϕ: Volume fraction, β: Fluid-particle interaction parameter, g (m/s^2): Acceleration due to gravity, C_p , C_m (J kg^{-1}K^{-1}): Specific heat of fluid and dust particles respectively, τ_T (s): Thermal equilibrium time, τ_v (s): Relaxation time of the dust particles, q''' $\left(\frac{\mathrm{K}}{\mathrm{m}^2}\right)$: Space and temperature dependent internal heat generation (non-uniform heat source/sink), k (W/mK): Thermal conductivity, ϑ (m^2/s): Kinematic viscosity of the fluid, A^*, B^*: Coefficient of space and temperature-dependent internal heat generation/absorption respectively, T_w, T_∞ (K): Temperature at the wall and at a large distance respectively, T, T_p (K): Temperature of fluid and dust particles respectively, γ: Curvature parameter, Gr: Local Grashof number, Q: Magnetic parameter, S: Permeability parameter, l^* (kg/m^3): Mass concentration of dust particles, E: Volume fraction parameter, Pr: Prandtl number, Ec: Eckert number, a_1: Local fluid-particle interaction parameter of temperature, a_2: Local fluid-particle interaction parameter of velocity, b_1: Specific heat parameter, ω: Density ratio, A, D: Constants, $U_w(z)$ (m/s): Stretching velocity, b (s^{-1}): Stretching rate, l (m): Reference length. a (m): Radius of the cylinder, η: Similarity variable, $\rho_r(= \rho_p/\rho)$: Relative density, Re_x: Local Reynolds number.

REFERENCES

Chakrabarti, K.M. (1977) Note on the boundary layer in a dusty gas. *American Institute of Aeronautics and Astronautics Journal*. **12,** 1136-1137.

Chang, C.L. (2008) Numerical simulation for natural convection of micropolar fluids along slender hollow circular cylinder with wall conduction effect. *Communication in non-linear Science and Numerical Simulation*. **13,** 624-636.

Dey, D. (2016a) Dusty hydromagnetic Oldroyd fluid flow in a horizontal channel with volume fraction and energy dissipation. *International Journal of Heat and Technology.* **34**, 415-422.

Dey, D. (2016b) Non-Newtonian effects on hydromagnetic dusty stratified fluid flow through a porous medium with volume fraction. *Proceedings of the National Academy of Sciences, India Section A: Physical Sciences.* **86**, 47-56.

Dey, D. and Chutia, B. (2020) Dusty nanofluid flow with bioconvection past a vertical stretching surface. *Journal of king Saud University- Engineering Sciences.* In press.

Dey, D. and Hazarika, M. (2020) Entropy Generation of Hydro-Magnetic stagnation point flow of micropolar fluid with energy transfer under the effect of uniform suction/ injection. *Latin American Applied Research.* **50**, 209-214.

Dey, D. and Borah, R. (2020) Dual solutions of boundary layer flow with heat and mass transfers over an exponentially shrinking cylinder: stability analysis. *Latin American Applied Research.* **50,** 247-253.

Gireesha, B.J., Chamkha, A.J., Manjunatha, S. and Bagewadi, C.S. (2013) Mixed convective flow of a dusty fluid over a vertical stretching sheet with non-uniform source/sink and radiation. *Interna-tional Journal of Numerical Methods for Heat and fluid flow*. 23, 598-612.

Gupta, R.K and Gupta, K. (1990) Unsteady Flow of a dusty visco-elastic fluid through channel with volume fraction. *Indian Journal of Pure and Applied Mathematics*, **21,** 677-690.

Manjunatha, P.T., Gireesha, B.J. and Prasannakumara, P.C. (2014) Thermal analysis of conducting dusty fluid flow in porous medium over-stretching cylinder in the presence of non-uniform source/sink. *International Journal of Mechanical and Materials Engineering*. **9,** 1-13.

Mucoglu, A. and Chen, T.S (1975) Buoyancy effects on forced convection along a vertical cylinder with uniform surface heat flux. *Journal of heat transfer*.**98,** 523-525.

Nayfeh, J. and Vajravelu, K. (1992) Hydromagnetic flow of a dusty fluid over a stretching sheet. *International Journal of non-linear Mechanics*. **27,** 937-945.

Prasad, K.V., Vajravelu, K., Vaidya, H. and Santhi, S.R. (2016a) Axisymmetric flow of a Nanofluid past a vertical slender cylinder in the presence of a transverse magnetic field. *Journal of Nanofluid.* **5,** 101-109.

Prasad, K.V., Vajravelu, K., Shivakumara, I.S., Vaidya, H. and Barsha, Neelufer.Z. (2016b) Flow and Heat transfer of a Casson Nanofluid over a Non-linear Stretching Sheet. *Journal of Nanofluid.* **5,** 743-752.

Prasad, K.V., Vaidya, H., Makinde, O.D., Vajravelu, K. And Ramajini, V. (2020) Impact of suction/injection and heat transfer on unsteady MHD flow over a stretchable rotating disk. *Latin American Applied Research.* **50**, 159-165.

Saffman, P.G. (1962) On the stability of laminar flow of a dusty gas. *Journal of Fluid Mechanics*. **13,** 120-128.

Singh, N.P. and Singh, A.K. (2002) MHD effects on convective flow of a dusty viscous fluid and volume fraction. *Bulletin of the Institute of Academia Sinica*. **30,** 141-151.

Vaidya, H., Rajashekhar, C., Manjunatha, G., Prasad, K. V., Makinde O. D. and Vajravelu, K. (2020) Heat and mass transfer analysis of MHD peristaltic flow through a complaint porous channel with variable thermal conductivity. *Physica Scripta*, **95**, 045219.

Vaidya, H., Prasad, K.V., Tlili, I., Makinde, O.D., Rajashekhar, C., Khan, S.U., Kumar, R. And Mahendra, D.L. (2021) Mixed convective nanofluid flow over a non-linearly stretched Riga plate. *Case studied in Thermal Engineering.* **24**, 100828.

Wang, C.Y. (1988) Fluid flow due to a stretching cylinder. *Physics of Fluids*. **31**, 466-468.

Received: July 4, 2020
Sent to Subject Editor: January 13, 2021
Accepted: April 9, 2021
Recommended by Subject Editor Gianfranco Caruso